Journal of Functional Foods 107 (2023) 105642

Contents lists available at ScienceDirect

Journal of Functional Foods

journal homepage: www.elsevier.com/locate/jff

Hepatoprotective effect of cyanidin-3-*O*-glucoside–lauric acid ester against H_2O_2-induced oxidative damage in LO2 cells

Ping Zhou [a,1], Ying Pan [b,1], Wei Yang [c,d], Baoru Yang [d], Shiyi Ou [a], Pengzhan Liu [e,*], Jie Zheng [a,*]

[a] Department of Food Science and Engineering, Jinan University, Guangzhou, Guangdong 510632, China
[b] Department of Obstetrics and Gynecology, the First Affiliated Hospital of Jinan University, Guangzhou 510632, Guangdong, China
[c] School of Food Science and Technology, Collaborative Innovation Center of Food Safety and Quality Control in Jiangsu Province, Jiangnan University, 1800 Lihu Road, Wuxi, Jiangsu 214122, China
[d] Food Chemistry and Food Development, Department of Biochemistry, University of Turku, Turku FI-20014, Finland
[e] School of Food Science and Engineering, South China University of Technology, Guangzhou, Guangdong 510641, China

ARTICLE INFO

Keywords:
Anthocyanin
Fatty acid esterification
LO2 cells
Antioxidation
Hepatoprotection

ABSTRACT

Acylation of anthocyanin with fatty acid has been extensively applied for the improvement of their lipophilicity and stability. However, their functionalities are not fully investigated. This work prepared cyanidin-3-*O*-glucoside–lauric acid ester (C3G–LA) and investigated its protective effect against oxidative stress in H_2O_2-induced human normal liver (LO2) cells. The results indicated that C3G–LA possessed notable antioxidant activity and better protective effect than its anthocyanin precursor cyanidin-3-*O*-glucoside (C3G). It protected the cells from H_2O_2-induced cell death and apoptosis by suppressing the overproduction of reactive oxygen species and malondialdehyde, restoring superoxide dismutase activity and ameliorating mitochondrial dysfunction and membrane damage. The increase in the expression levels of phosphorylated Akt, Nrf2, HO-1 and NQO1 further indicated that the antioxidant protective effect of C3G–LA involved the PI3K/Akt-mediated activation of the Nrf2–HO-1/NQO1 pathway. The findings indicated that, in addition to improve lipophilicity and stability, acylation of anthocyanin can enhance their anti-oxidative stress activity.

1. Introduction

Anthocyanins are the most common and widely distributed flavonoids responsible for the vivid blue, red and purple colours of various plant structures, such as fruits, flowers and leaves. They possess numerous health-promoting properties, including antioxidant effect, antimicrobial properties (Gong et al., 2021), anti-diabetic and anti-obesity effects (Tian et al., 2021; Teixeira et al., 2021), neuroprotective effect (Li et al., 2020), anti-hypolipidemic effect (Ershad, Shigenaga, & Bandy, 2021) and anti-tumour activity (Wei et al., 2021); alleviate osteoarthritis (Jiang et al., 2019) and vision complications (Nomi, Iwasaki-Kurashige, & Matsumoto, 2019) and prevent cardiovascular diseases (Wood, Hein, Heiss, Williams, & Rodriguez-Mateos, 2019). All of these extraordinary health-promoting properties have brought much interest to the study of anthocyanins, and promoted their application as functional ingredients in the food, cosmetics and pharmaceutical fields, as well as their application as natural alternatives to artificial food colourants (Sinopoli, Calogero, & Bartolotta, 2019). However, the utilisation of anthocyanins as food colourants and functional ingredients are still largely limited due to their low stability and poor solubility in lipophilic food matrix.

Acylation is a potential pathway to improve the stability of anthocyanins (Zeng et al., 2021). In the last decades, enzymatic acylation of anthocyanin with fatty acid has been extensively applied in order to improve the lipophilic solubility and stability. Various anthocyanins, including cyanidin-3-*O*-glucoside (C3G) (Guimarães et al., 2019), cyanidin-3-*O*-galactoside (Yang, Kortesniemi, Yang, & Zheng, 2018), delphinidin-3-*O*-glucoside (Cruz et al., 2018), cyanidin-3-*O*-rutinoside, delphinidin-3-*O*-rutinoside (Yang, Kortesniemi, Ma, Zheng, & Yang, 2019), delphinidin-3-*O*-sambubioside (Marquez-Rodriguez et al., 2021) and malvidin-3-*O*-glucoside (Cruz et al., 2017), have been successfully esterified with fatty acids of different chain lengths. In addition to enhance their stability, acylation also improves the lipophilicity of anthocyanins, and the acylated anthocyanins show great potential for

* Corresponding authors.
E-mail addresses: lpzhan@scut.edu.cn (P. Liu), zhengjie@jnu.edu.cn (J. Zheng).
[1] Zhou P and Pan Y have contributed equally to this work.

https://doi.org/10.1016/j.jff.2023.105642
Received 7 April 2023; Received in revised form 15 June 2023; Accepted 19 June 2023
Available online 25 June 2023

application in lipophilic food mediums (Guimarães et al., 2019; Yang et al., 2019; Marquez-Rodriguez et al., 2021; Cruz et al., 2017; Zhang et al., 2021). Moreover, the toxicological evaluation of anthocyanin–lauric acid derivatives proved the enzymatic acylation as a safety way for preparation of acylated anthocyanins (Yang et al., 2020).

Antioxidant capacity is one of the most valued and focused bioactive characteristics of the acylated products of anthocyanins for application as antioxidants in food, cosmetics and pharmaceuticals. However, different *in vitro* assays, such as 2,2-diphenyl-1-picrylhydrazyl radical scavenging capacity assay, ferric-reducing antioxidant power assay and β-carotene bleaching assay, gave inconsistent results in antioxidant capacity evaluation (Yang et al., 2018; Yang et al., 2019; Zhang et al., 2021). These methods have been widely announced to be non-specific and highly prone to interferences, and hardly related to health outcomes. Moreover, it has become extensively questioned whether the health benefits of a compound that is *in vitro* antioxidants arise from their *in vivo* antioxidant activity (Harnly, 2017). In comparison with chemical-based antioxidant activity assays, cellular investigations include cellular adsorption, metabolism and intracellular distribution of antioxidants, which provide a more accurate and representative evaluation of the biological activity of food ingredients. Moreover, investigations on the compound against cellular oxidative stress and damage could further provide information on the underlying mechanism involved in the protective effects of the compounds *in vivo*.

This work used C3G, which is one of the most widespread anthocyanins in nature, typically in coloured fruits, vegetables and especially in black soybean hulls (Gonçalves, Nunes, Falcão, Alves, & Silva, 2021; Jhan et al., 2016) to enzymatically prepare cyanidin-3-*O*-glucoside–lauric acid ester (C3G–LA). We intend to investigate protective effect of C3G–LA against oxidative stress induced by H_2O_2 in human normal liver (LO2) cells by comparison with its precursor C3G and vitamin E (VE) as the positive control, and to elucidate the hepatoprotective mechanisms of C3G–LA through the evaluation of the mitochondrial membrane potential, extracellular lactate dehydrogenase (LDH) level, intracellular reactive oxygen species (ROS) level, malondialdehyde (MDA) level and superoxide dismutase (SOD) activity. Furthermore, the expression of proteins involved in the apoptotic pathway and the PI3K/Akt and Nrf2–HO-1/NQO1 pathways were determined by Western blot analysis to explore the impact of C3G-LA on antioxidant signalling pathways.

2. Materials and methods

2.1. Materials and reagents

Crude anthocyanin extract from black bean hulls containing 35.8 % C3G was purchased from BGG Co., Ltd. (Beijing, China). *Candida antarctica* lipase B (Novozyme 435) was purchased from Chengdu Jian Quan Biological Technology Co., Ltd (Sichuan, China). Lauric acid (LA), 4 Å molecular sieves and C3G (98 %) were purchased from Energy Chemical (Shanghai, China). N,N-dimethylformamide (DMF), *tert*-butanol, ethyl acetate, formic acid and dichloromethane were analytical grade and purchased from Guangzhou Lubex Biological Technology Co., Ltd. (Guangdong, China). Column chromatography silica gel (200–300 mesh) was obtained from Qingdao Ocean Chemical Co., Ltd. (Qingdao, China). Human normal liver cell (LO2 cells) was obtained from iCell Bioscience, Inc. (Shanghai, China). RPMI 1640 medium, foetal bovine serum, penicillin and streptomycin were purchased from Thermo Fisher Scientific (Shanghai, China). Primary antibodies against Bax (2772), Bcl-2 (15071), AKT (4691), Nrf2 (16236), p-AKT (4060), NQO1 (6437), HO-1 (5393) and GAPDH (5174), as well as horseradish peroxidase (HRP)-conjugated anti-rabbit IgG (7074) as the secondary antibody, were obtained from Cell Signalling Technology (Danvers, MA, USA).

2.2. Preparation and purification of C3G–LA

The molecular sieve was activated at 150 °C for 24 h before use. The reaction media of 10 % DMF in *tert*-butanol was dried with the molecular sieves (100 mg/mL) overnight. Crude anthocyanin extract (3 g) from black bean hulls and LA (4.8 g) were dissolved in 50 mL reaction media containing 5 g molecular sieve. The reaction was started by adding Novozyme 435 (10 g/L) and continued by magnetic stirring at 60 °C for 72 h (Zhou et al., 2021). The reaction was terminated by filtering through a 0.45 μm nylon filter membrane to remove the molecular sieve and the enzyme. *tert*-Butanol was evaporated by a rotary vacuum evaporator under 45 °C. The residues were dissolved in a mixture of 20 mL NaCl-saturated solution, 20 mL $NaHCO_3$-saturated solution and 50 mL ethyl acetate. C3G–LA was collected in the ethyl acetate phase, whereas C3G was left in aqueous phase. Liquid–liquid extraction by ethyl acetate was conducted until the ethyl acetate phase turned colourless. After ethyl acetate was evaporated, the C3G–LA extract was further purified with a chromatographic column filled with silica and eluted with gradient solutions of dichloromethane/methanol/formic acid at the volume ratios of 20:1:1 (420 mL), 15:1:1 (340 mL), 13:1:1 (560 mL) and 10:1:1 (200 mL). The fraction that comprised C3G–LA with over 95 % purity was collected and dried under reduced vacuum. The purified product was kept at –20 °C.

2.3. Structural verification

The purified acylated anthocyanin product was dissolved in CD_3OD acidified with 5 % CF_3COOD and characterised by ^1H and ^{13}C nuclear magnetic resonance (NMR) analyses with an Avance III HD 600 NMR spectrometer (Bruker, Fällanden, Switzerland).

2.4. Cell culture and treatments

LO2 cells were cultivated the same way as described by Yin et al. (Yin et al., 2020). After cultivation, the cells were detached with 0.25 % trypsin–EDTA and harvested. The H_2O_2-induced oxidative damage model of LO2 cells was established through the determination of H_2O_2 treatment level that leads to the death of approximately half of the cells. For this purpose, LO2 cells were treated with H_2O_2 at concentrations of 0, 0.2, 0.25, 0.5, 1, 2, 4 and 6 mM at 37 °C for 6 h, and then cell viability was evaluated. Once the administration level of H_2O_2 was determined, the hepatoprotective effect of C3G–LA was investigated. The LO2 cells were treated with different concentrations of C3G–LA and C3G (10, 50, 100, 200 and 300 μM) for 24 h and incubated with H_2O_2 to induce oxidative stress in the cells. The two groups of LO2 cells set as positive and negative controls were respectively treated with VE (200 μM) and culture medium containing 1 % dimethyl sulfoxide (DMSO) for 24 h and then treated with H_2O_2. The cells cultivated for 30 h without any treatment was used as blank control. C3G–LA and C3G were first dissolved in DMSO at a concentration of 50 mM and then diluted to the desired concentrations in the culture medium for administration.

2.5. Cell viability assays

Cell viability was measured by MTS assay using the CellTiter 96® AQ_{ueous} One Solution Cell Proliferation Assay Kit (Madison, WI, USA) according to the manufacturer's instructions. LO2 cells were seeded in a 96-well plate (Corning Scientific, USA) at a density of 1×10^4 cells/well and incubated at 37 °C for 24 h and underwent different treatments as described in Section 2.4. After the treatments, the culture medium was removed, the cells were washed with 100 μL of PBS and refilled with 180 μL of culture medium. MTS reagent (20 μL) was then added to each well and incubated at 37 °C for 4 h. The absorbance of the samples was finally measured at 490 nm using a microplate reader (EPOCH2, BioTek, VT, USA).

2.6. Apoptosis analysis

LO2 cells were seeded in a 6-well plate (Corning Scientific, USA) at a density of 2–5 × 10^5 cells/well, incubated at 37 °C for 24 h, then underwent different treatments with 1 %DMSO, VE (200 μM), C3G–LA (50 and 200 μM) and C3G (50 and 200 μM) for 24 h, and incubated with H_2O_2 (200 μM) for 6 h. The double dye Annexin V–fluorescein isothiocyanate (FITC)/propidium iodide (PI) were used to study the apoptosis rate of LO2 cells after different treatments. The treated cells were harvested with EDTA-free trypsin, washed twice with 2 mL of cold PBS and resuspended in the binding buffer. Cells were stained with Annexin V–FITC/PI according to the protocol of the Annexin V–FITC/PI Apoptosis Detection Kit (Becton, Dickinson and Company, NJ, USA). The fluorescence intensity of the stained cells was measured by a BD FACSCanto flow cytometer (BD Biosciences, San Jose, USA).

2.7. Determination of LDH release

LO2 cells were seeded in a 6-well plate (Corning Scientific, USA) at a density of 2–5 × 10^5 cells/well and treated as described in Section 2.6. LDH release was analysed using a LDH enzyme-linked immunosorbent assay (ELISA) kit according to the instructions of the manufacturer. Briefly, the treated cells were centrifuged, and the supernatant of the cell culture medium was collected. The sample was incubated with 100 μL of HRP conjugate at 37 °C for 1 h, washed five times, incubated with substrate reagents at 37 °C for 15 min and added with stop solution. The signals were finally detected within 15 min at 450 nm using a microplate reader (EPOCH2, BioTek, VT, USA).

2.8. Determination of intracellular ROS level

Dichloro-dihydro-fluorescein diacetate (DCFH-DA) assay was applied to determine the generation of intracellular ROS in oxidatively stressed cells by H_2O_2 stimulation. LO2 cells were seeded in a 6-well plate (Corning Scientific, USA) at a density of 2–5 × 10^5 cells/well and treated as described in Section 2.6. The assay was performed using the Reactive Oxygen Species Assay Kit (Beyotime, Shanghai, China) following the instructions provided by the manufacturer. In brief, the treated cells were washed twice with cold PBS and stained with DCFH-DA for 15 min in the dark. Afterwards, the cells were washed with PBS, resuspended in 300 μL of PBS and analysed by flow cytometry.

2.9. Mitochondrial membrane potential (MMP) analysis

LO2 cells were seeded in a 6-well plate (Corning Scientific, USA) at a density of 2–5 × 10^5 cells/well and treated as described in Section 2.6. The treated cells were collected, washed twice with cold PBS and stained with 200 μL of JC-1 staining buffer (Becton, Dickinson and Company, NJ, USA) for 15 min at 37 °C in the dark. The stained cells were then washed with PBS, resuspended in 300 μL of PBS and measured by flow cytometry.

2.10. Determination of MDA level and SOD activity

The MDA content and SOD activity were measured using commercially available MDA and SOD ELISA kits (Sinobestbio, Shanghai, China) in accordance with the manufacturer's protocol. LO2 cells were seeded in a 6-well plate (Corning Scientific, USA) at a density of 2–5 × 10^5 cells/well and treated as described in Section 2.6. The cells were harvested, washed with cold PBS, lysed with radioimmunoprecipitation assay (RIPA) lysis buffer (Promega Corporation, WI, USA) and centrifuged. The supernatant was obtained for MDA content and SOD activity assays. The absorbance was measured using a microplate reader (EPOCH2, BioTek, VT, USA) at 450 nm.

2.11. Western blot analysis

LO2 cells were seeded in a 6-well plate (Corning Scientific, USA) at a density of 2–5 × 10^5 cells/well and treated as described in Section 2.6. The treated cells were harvested, washed twice with cold PBS and lysed in whole cell lysis buffer (RIPA lysis buffer, Promega Corporation, WI, USA). The protein was extracted following the addition of proteinase inhibitor. Equivalent amounts of protein were separated by sodium dodecyl sulphate–polyacrylamide gel electrophoresis, transferred onto polyvinylidene fluoride (PVDF) membranes and blocked with skim milk for 1 h. The PVDF membranes were washed with Tris-buffered saline–Tween 20 (TBST) for 5 min and incubated with the corresponding primary antibody at 4 °C overnight. Thereafter, the membranes were washed thrice with TBST for 10 min, incubated with HRP-conjugated goat anti-rabbit IgG at 37 °C for 1 h and analysed with Bio-Rad Chem-iDoc MP imaging system (Bio-Rad Laboratory, Hercules, CA, USA). The intensities of protein bands were quantified by ImageJ software (National Institutes of Health, USA) with GAPDH as the loading control.

2.12. Statistical analysis

Statistical analyses were conducted by SPSS Statistics 25.0 (SPSS, Inc., Chicago, IL, USA). All the analyses were conducted in triplicates. Data are presented as mean ± SD. One-way ANOVA and Duncan's test were applied to determine the differences between samples at a significance level of 0.05.

3. Results and discussions

3.1. Structural verification of C3G–LA

C3G–LA was prepared by enzymatical acylation of crude anthocyanin extract from black bean hulls, followed by extraction and purification. The structure of the product was determined by ^{1}H and ^{13}C NMR analyses and chemical shifts detected are listed below.

^{1}H NMR (600 MHz, CD_3OD:CF_3COOD [95:5, v/v]): δ 8.90 (s, 1H, H-4), 8.24 (dd; J = 9.0, 2.4 Hz; 1H; H-6′), 8.00 (d, J = 2.4 Hz, 1H, H-2′), 7.01 (d, J = 8.7 Hz, 1H, H-5′), 6.88 (dd; J = 5.5, 1.1 Hz; 1H; H-8), 6.65 (d, J = 1.5 Hz, 1H, H-6), 5.29 (d, J = 7.8 Hz, 1H, H-1″), 4.43 (dd; J = 12.0, 1.8 Hz; 1H; H-6″a), 4.19 (dd; J = 12.0, 7.2 Hz; 1H; H-6″b), 3.76 (t/s, J = 6.6 Hz, 1H, H-5″), 3.66 (t, J = 8.4 Hz, 1H, H-2″), 3.53 (t, J = 9.3 Hz, 1H, H-3″), 3.39 (t, J = 9.3 Hz, 1H, H-4″), 2.27 (td; J = 7.2, 3 Hz; 2H; –C<u>H</u>$_2$–CO–), 1.46 (m, 2H, –C<u>H</u>$_2$–CH$_2$–CO–), 1.04–1.34 (m, 16H, –CH$_2$–lauroyl backbone), 0.84 (t, J = 7.5 Hz, 3H, –CH$_3$).

^{13}C NMR (150 MHz, CD_3OD:CF_3COOD [95:5, v/v]): δ 174.03 (C = O), 169.07 (C7), 163.10 (C2), 157.72 (C9), 156.25 (C5), 154.66 (C3), 146.15 (C3′), 144.06 (C4′), 135.1 (C4), 129.43 (C6′), 127.07 (C1′), 119.76 (C10), 116.98 (C2′), 116.02 (C5′), 102.02 (C6), 101.97 (C1″), 93.79 (C8), 76.42 (C5″), 74.58 (C3″), 73.21 (C2″), 70.03 (C4″), 63.15 (C6″), 33.42 (–C<u>H</u>$_2$–CO–), 22.29–31.63 (–CH$_2$–lauroyl backbone), 12.98 (–CH$_3$).

According to the data, the product was verified to be cyanidin-3-(6″-dodecanoyl)-glucoside, an esterified product of C3G with acylated LA at the 6″–OH of the glucoside moiety, as that previously prepared by our laboratory (Yang et al., 2019).

3.2. Protective effects of C3G–LA against H_2O_2-induced oxidative injury in LO2 cells

Oxidative stress is a crucial initiating factor that contributes to the pathogenesis of various diseases, such as hepatopathies and cardiovascular diseases (Poljsak, Šuput, & Milisav, 2013). Liver, being the central organ responsible for nutrient metabolism and detoxification, is vulnerable to damages induced by pathological factors, such as oxidative stress (Li et al., 2015). H_2O_2 is one of the main ROS that cause lipid peroxidation and DNA damage, which induce cellular apoptosis (Je &

Lee, 2015). It creates oxidative stress in normal human hepatocytes, similar to which occur in the intact liver. Therefore, H_2O_2-stressed LO2 cells are widely used to mimic oxidative stress-induced injury in the liver (Lu, Zhang, Hu, & Lu, 2014). The present study investigated the hepaprotective effect of the fatty acid-esterified anthocyanin C3G–LA by evaluating its protective effect against H_2O_2-induced oxidative damage in LO2 cells and elucidating the underlying mechanism of its effect. The cellular oxidative injury models of LO2 cells were established by exposing the cells to H_2O_2 with different concentrations for 6 h, after which the cell viability was measured. As shown in Fig. 1**A**, H_2O_2 treatment markedly inhibited cell proliferation in a dose-dependent manner. When the cells were exposed to 200 μM H_2O_2, their viability decreased to 51 % ($p < 0.05$). A further increase in the concentration of H_2O_2 gradually reduced cell viability to a minimum of 23 % at 2 mM. Thus, the H_2O_2 concentration of 200 μM was finally chosen for the establishment of oxidative injury in LO2 cells.

The protective effects of C3G–LA against H_2O_2-induced oxidative injury in LO2 cells were investigated in comparison to the impacts of C3G. As shown by Fig. 1**B**, when the cells were pretreated with 10 μM C3G–LA, the viability of LO2 cells was significantly elevated by 16 % ($p < 0.05$). In comparison, pretreatment with 10 μM C3G did not significantly impact on restoring the cell viability reduced by H_2O_2. C3G only displayed protective effect against H_2O_2-induced cellular damage at treatment levels over 50 μM. According to the statistical comparison (Fig. 1**B**), C3G–LA displayed a considerably better protective ability than C3G at the administration levels of 10–100 μM. Once the treatment level was over 200 μM, the two compounds displayed similar ($p > 0.05$) protective activities. Cell preincubation with 300 μM C3G and C3G–LA elevated the cell viability by 61 % and 63 %, respectively. These results indicated that pretreatment with C3G–LA could protect LO2 cells against H_2O_2-induced oxidative injury and reduce cell death. Given the remarkable protective potential of C3G–LA against oxidative stress, the underlying mechanism involved was further investigated. The administration levels of 50 and 200 μM were selected for the investigation.

3.3. C3G–LA inhibited H_2O_2-induced cellular apoptosis

H_2O_2 treatment dramatically enhanced apoptosis of LO2 cells (Fig. 2**A**). The population of apoptotic cells increased substantially from 7.9 % in the blank control group to 13.8 % under the treatment of 200 μM H_2O_2 for 6 h. This result suggested that H_2O_2 impaired LO2 cells and reduced their viability through apoptosis induction. Pretreatment with C3G–LA for 24 h prior to H_2O_2 exposure significantly protected the cells and attenuated the cellular apoptosis rate by 20 % and 24 % under the C3G–LA treatment levels of 50 and 200 μM, respectively. In comparison, pre-incubation with 50 and 200 μM C3G reduced the H_2O_2-induced apoptosis rate by 9 % and 17 %, respectively. Overall, C3G–LA showed a better protective effect against H_2O_2-induced apoptosis than C3G, although no significant differences ($p > 0.05$) were observed between the two compounds at the same administration level.

Western blot analyses were performed to evaluate the expression levels of the apoptotic markers Bax and Bcl-2. Bcl-2 family members play an important role in the regulation of cellular apoptosis (Vander Heiden, Chandel, Williamson, Schumacker, & Thompson, 1997). Amongst them, the anti-apoptotic protein Bcl-2 and the pro-apoptotic protein Bax are the most important and the most investigated proteins, as their interactions may influence cell fate. They are considered the principal factors that determine the progress of apoptosis. As shown in Fig. 2**B**, the administration of H_2O_2 induced a 2.4-fold increase in Bax expression and an 85 % decrease in Bcl-2 expression. Pretreatment with 50 and 200 μM C3G–LA remarkably downregulated the expression level of Bax by 33 % and 81 %, respectively, in H_2O_2-treated LO2 cells. The expression level of Bax was significantly lower ($p < 0.05$) in the cells preincubated with 200 μM C3G–LA for 24 h than those treated with the same level of C3G and was statistically equivalent ($p > 0.05$) to the positive control group treated with VE. Pretreatment with 50 μM C3G–LA did not show an impact on the expression level of anti-apoptotic Bcl-2 ($p > 0.05$). Whereas, when the treatment level was increased to 200 μM, the expression level of Bcl-2 was upregulated by 1.4 folds ($p < 0.05$). The Bcl-2/Bax ratio is critical for the determination of the onset of cell apoptosis (Bai, Zheng, Wang, & Liu, 2016). A decrease in Bcl-2/Bax ratio promotes the release of cytochrome *c* from the mitochondria into the cytosol and subsequently leads to caspase activation (Thornberry & Lazebnik, 1998). As shown in Fig. 2**C**, the Bcl-2/Bax ratio was markedly lowered from 1.50 in the blank control to 0.06 in the cells treated with H_2O_2, whereas pretreatment with 200 μM C3G–LA elevated the Bcl-2/Bax ratio to 0.97, which was similar to that of the positive control (VE). The results indicated that Bcl-2 family proteins play a critical role in H_2O_2-induced apoptosis, and C3G–LA could protect LO2 cells against H_2O_2-induced apoptosis by regulating the expression levels of Bcl-2 and Bax.

3.4. C3G–LA reduced LDH release

LDH is always released to the surrounding extracellular space when the cell membrane is damaged, and LDH can be easily detected in the culture medium (Jian et al., 2018). The release of LDH indicates the impairment of plasma membrane integrity and demonstrates the cytotoxicity of the compound towards the cells (Shi & Zhao, 2019). As shown in Fig. 3, H_2O_2 treatment caused a 2.1-fold increase in LDH release compared with the control group ($p < 0.05$), which indicated the markedly loss of membrane integrity. In comparison, pretreatment with

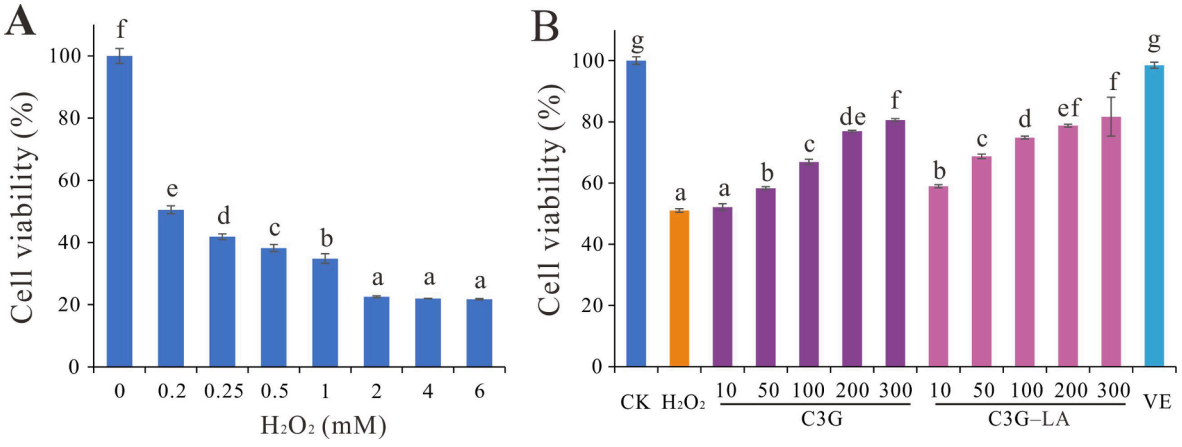

Fig. 1. Cell viability under treatments of different concentrations of $H_2O_{2\ (0.2–6\ mM)}$ (A) and different treatments of C3G (50, 200 μM), C3G-LA (50, 200 μM) and VE (200 μM) prior to H_2O_2 (200 μM) exposure (B). Different letters indicate significant differences ($p < 0.05$) between treatments.

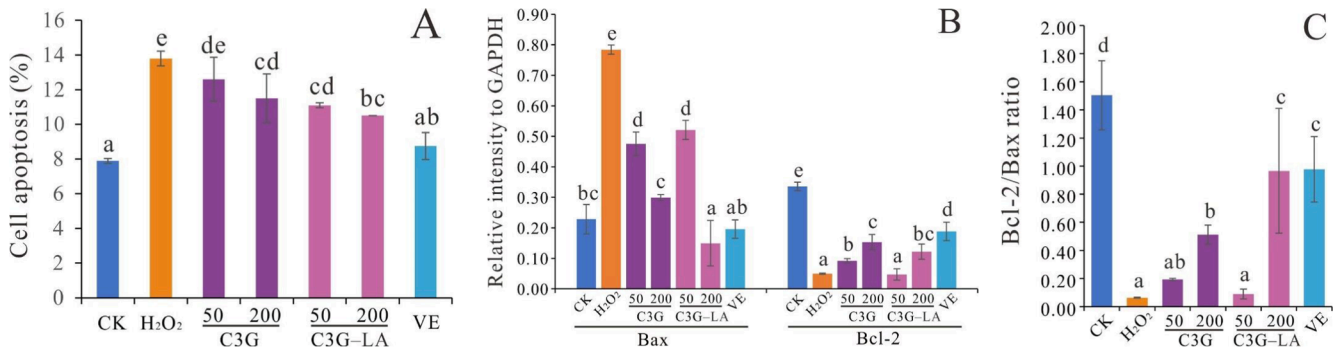

Fig. 2. Protective effects of treatments of C3G (50, 200 μM), C3G–LA (50, 200 μM) and VE (200 μM) on the H_2O_2-induced apoptosis of LO2 cells (A) and their impacts on the expression of apoptotic markers (B) and Bcl-2/Bax ratio (C). Different letters indicate significant differences ($p < 0.05$) on the corresponding determination parameter between treatments.

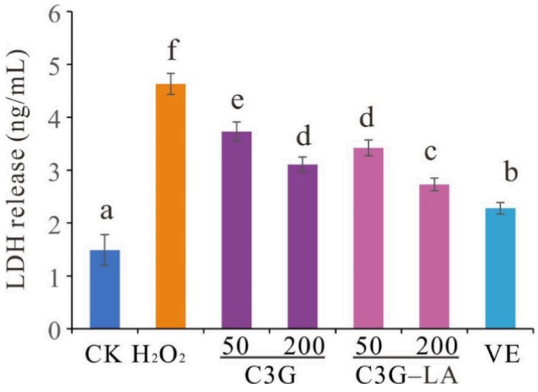

Fig. 3. The inhibitory effects of C3G (50, 200 μM), C3G–LA (50, 200 μM) and VE (200 μM) on the LDH release of H_2O_2-induced LO2 cells. Different letters on the column indicate significant differences ($p < 0.05$) between treatments.

C3G–LA and C3G remarkably reduced LDH release by 39 % and 19 % at the administration level of 50 μM and by 56 % and 41 % at the treatment level of 200 μM, respectively. Moreover, C3G–LA displayed a better protective effect than C3G on the H_2O_2-stressed cells. This result is consistent with the results of the cell viability analyses.

3.5. C3G–LA suppressed H_2O_2-induced ROS overproduction

Oxidative stress is often associated with an enhanced production of reactive oxygen species (ROS). ROS are important signal mediators involved in the growth, differentiation, progression and death of cells under various physiological circumstances (Tang et al., 2018). The imbalance between the production and destruction of ROS will lead to oxidative stress injury and detrimental effects, which account for the cause or consequence of over 100 diseases, including liver diseases (Xia et al., 2017; Wang et al., 2018). In the current study, the DCFH-DA fluorescent probe was applied to determine the generation level of intracellular ROS in H_2O_2-stressed LO2 cells and its variation upon pretreatment with C3G–LA prior to H_2O_2 treatment. As shown in Fig. 4**A**, H_2O_2 induced the elevated production of ROS in the cells, which was 1.3 folds compared with that of the control group. Pretreatment with 50 and 200 μM C3G–LA remarkably attenuated the generation of ROS triggered by H_2O_2 treatment by 10.7 % and 13.5 %, respectively, which were almost comparable to the decrease level (by 15.9 %) under VE treatment. In comparison, the application of 50 μM C3G did not reverse the overproduction of ROS induced by H_2O_2, whereas 200 μM C3G reduced ROS generation by 10.7 %. The results implied that C3G–LA could protect LO2 cells from oxidative damage by inhibiting H_2O_2-induced ROS generation.

3.6. C3G–LA ameliorated H_2O_2-induced mitochondrial dysfunction

In mammalian cells, ROS are generated in the mitochondria. The excessive intracellular accumulation of ROS is believed to induce mitochondrial damage and MMP collapse, which are regarded as characteristics of early apoptosis (Xia et al., 2017; Circu & Aw, 2010). Therefore, MMP stabilisation is crucial and beneficial to maintain the normal physiological function of LO2 cells. The exposure of LO2 cells to 200 μM H_2O_2 resulted in a 26 % loss in MMP compared with the blank control (Fig. 4**B**). The loss in MMP may initiate the mitochondrial-mediated intrinsic apoptosis pathway. In accordance with the protective effect on cellular apoptosis, C3G–LA displayed an apparent protective effect on MMP stabilisation. Preincubation of cells with 50 and 200 μM C3G–LA elevated the MMP value by 13 % and 28 %, respectively, compared with sole H_2O_2 treatment. The protective effect on MMP by 200 μM C3G–LA was statistically comparable to that of the positive control group ($p > 0.05$). The results indicated that C3G–LA could restore H_2O_2-triggered MMP loss, ameliorate mitochondrial dysfunction and play a role in the protection through the ROS-mediated mitochondrial pathway.

3.7. C3G–LA suppressed H_2O_2-induced lipid peroxidation and elevated SOD activity

The variation level of the typical lipid peroxide marker MDA was also determined in H_2O_2-stressed cells applied with different protective treatments. MDA level notably increased by 1.3 folds under H_2O_2 treatment ($p < 0.05$, Fig. 5**A**). Pretreatments with C3G–LA and C3G showed remarkable suppressive effects on the overproduction of MDA in H_2O_2-treated cells. MDA is a degradative product of the oxidation of cell membrane lipids caused by excessive ROS accumulation; MDA denatures proteins and mutates DNA, which eventually lead to cell apoptosis (Xia et al., 2017). The increase in lipid peroxide reduces cell membrane fluidity and the activities of antioxidant enzymes within cells (Jian et al., 2018). As shown in Fig. 5**B**, H_2O_2 treatment markedly impaired SOD activity to less than half of that of the control, whereas pretreatment with C3G–LA prior to H_2O_2 treatment considerably prevented the decrease in SOD activity. Preincubation with 50 and 200 μM C3G–LA increased SOD activity by 30 % and 61 %, respectively, in the H_2O_2-stressed LO2 cells ($p < 0.05$). Nevertheless, these values still did not reach the level achieved in the positive control.

3.8. C3G–LA up-regulated PI3K/Akt-mediated Nrf2–HO-1/NQO1 pathways

The Nrf2–ARE signalling pathway has a major role in the cellular defence against oxidative stress. It regulates the expression of antioxidant genes and genes encoding phase II metabolic enzymes in the liver (Li et al., 2021). Therefore, Western blot was conducted to determine the

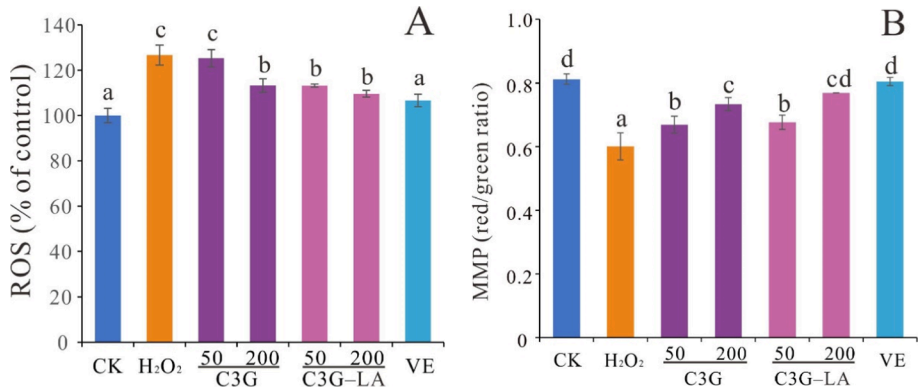

Fig. 4. The effects of C3G (50, 200 μM), C3G–LA (50, 200 μM) and VE (200 μM) on the levels of ROS (A) and MMP (B) of H_2O_2-injured LO2 cells. Different letters indicate significant differences ($p < 0.05$) between treatments.

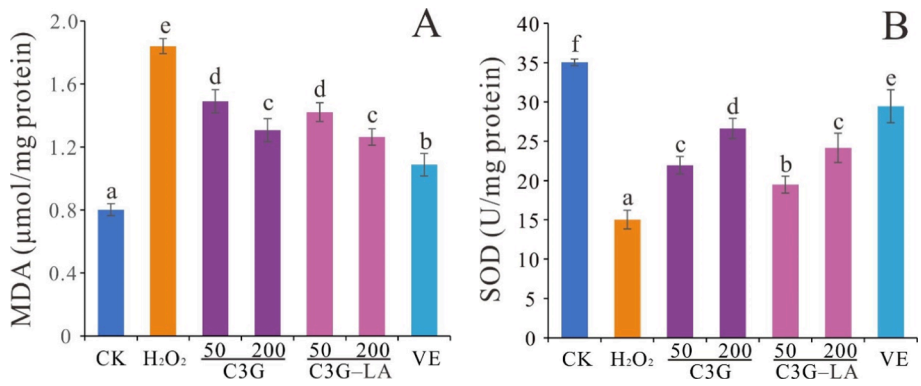

Fig. 5. The effects of C3G (50, 200 μM), C3G–LA (50, 200 μM) and VE (200 μM) on MDA level (A) and SOD activity (B) in H_2O_2-induced LO2 cells. Different letters indicate significant differences ($p < 0.05$) between treatments.

expression levels of Nrf2 and phase II detoxifying antioxidant enzymes, namely, HO-1 and NQO1, to further clarify the underlying antioxidant mechanisms of C3G–LA. HO-1 and NQO1 are crucial mediators in cells for maintaining antioxidant homeostasis in response to physiological stress. HO-1 is the key cytoprotective enzyme that catalyses the degradation of free heme to bilirubin; the latter serves as an endogenous antioxidant (Kensler, Wakabayashi, & Biswal, 2007). NQO1 plays an antioxidant protective role by catalysing the electron reduction of quinoid compounds using NADH and/or NADPH as electron donors (Martínez-Hernández et al., 2015). Nrf2 is recognised as a key transcription factor that adaptively regulates oxidative damage (Xia et al., 2017). The results showed that the expression levels of Nrf2, HO-1 and NQO1 decreased remarkably in response to H_2O_2 treatment (Fig. 6). Pretreatment with 50 μM C3G–LA hardly impacted the expression levels of Nrf2 and HO-1 but increased that of NQO1 by 2.8 folds. Administration with 200 μM C3G–LA prior to H_2O_2 exposure markedly elevated the expression levels of Nrf2, HO-1 and NQO1 by 0.5, 5.5 and 6.8 folds, respectively. These results indicated the activation of the Nrf2–HO-1/NQO1 pathway during antioxidant defence by C3G–LA treatment against H_2O_2-induced stress. Moreover, elevated Akt phosphorylation was detected as a result of C3G–LA treatment in H_2O_2-stressed LO2 cells (Fig. 6). The PI3K/Akt signalling pathway is involved in Nrf2-dependent transcription and consequent HO-1 expression in diverse cells in response to oxidative stress and different stimuli (Gao et al., 2018). Thus, the protective effect of C3G–LA against H_2O_2-induced oxidative injury involved the enhancement of Akt protein phosphorylation, which contributed to the activation of Nrf2 pathways and the expression of down-streamed antioxidants and phase II detoxifying enzymes.

4. Conclusion

C3G–LA displayed remarkable hepatoprotective effects against H_2O_2-induced oxidative damage in LO2 cells *via* the regulation of PI3K/Akt signalling pathway, and the consequent activation of Nrf2–ARE pathway. C3G–LA up-regulated the expression levels of Nrf2 and the downstream expression levels of NQO1 and HO-1 in H_2O_2-stressed LO2 cells, inhibited the excessive production of intracellular ROS and MDA, restored MMP, enhanced antioxidant enzyme activity, improved cell membrane integrity, inhibited cellular apoptosis and finally ameliorated cell survival and proliferation in response to the oxidative stress triggered by H_2O_2. The results indicated that C3G–LA may possess a better hepatoprotective effect than C3G and can be adopted as an alternative antioxidant food ingredient in the future.

Funding

This work was supported by the Guangdong Basic and Applied Basic Research Foundation (2021A1515012504); the Guangzhou Science Technology and Innovation Commission (201904010400); and the Foundation for Research of Natural Resources in Finland (2018001).

CRediT authorship contribution statement

Ping Zhou: Investigation, Methodology, Writing - original draft. **Ying Pan:** Investigation, Methodology, Writing – original draft, Supervision. **Wei Yang:** Data curation, Formal analysis, Validation. **Baoru Yang:** Supervision. **Shiyi Ou:** Conceptualization, Writing – review & editing. **Pengzhan Liu:** Data curation, Formal analysis, Funding acquisition, Supervision, Validation, Writing – review & editing. **Jie**

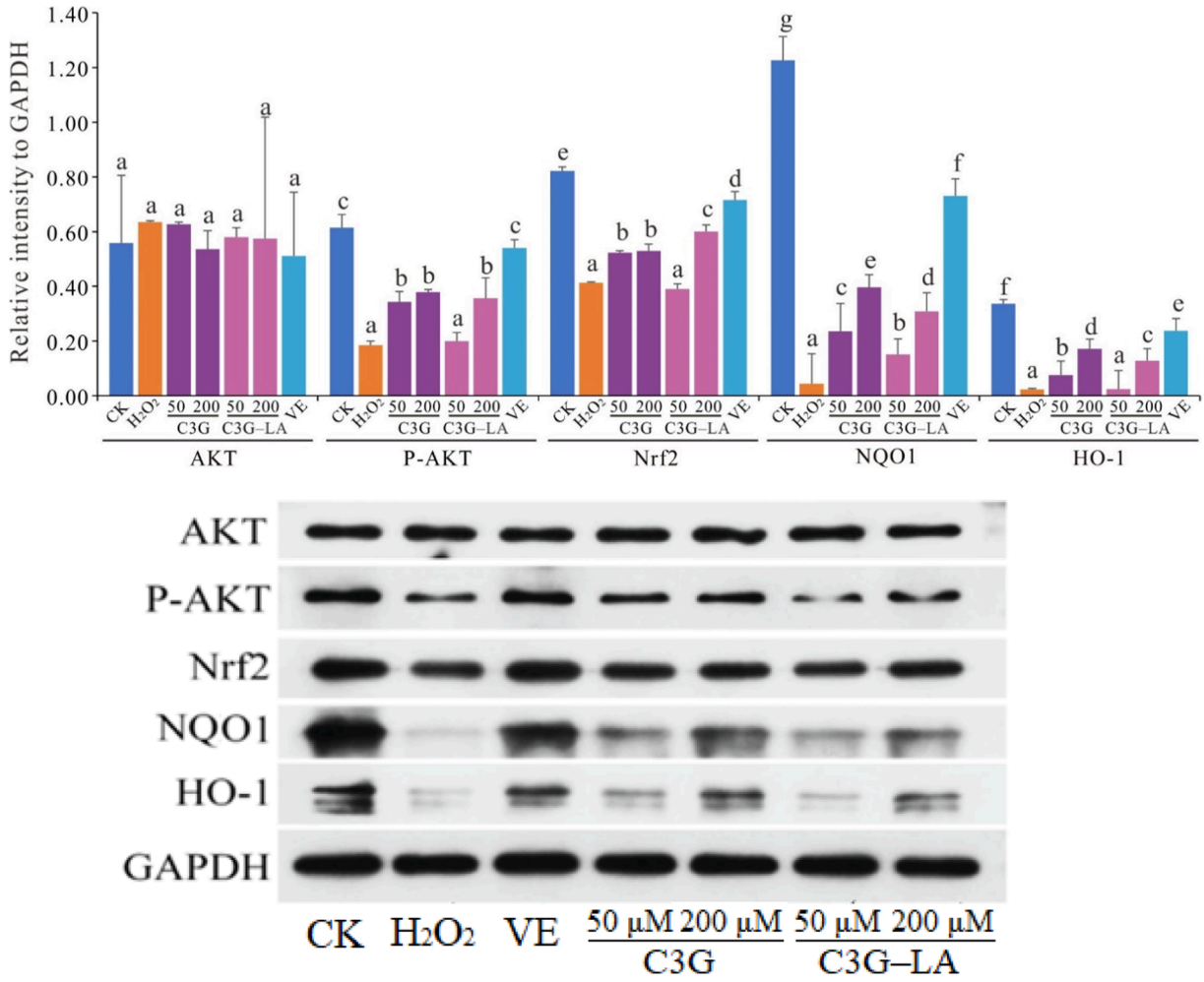

Fig. 6. The effects of C3G (50, 200 μM), C3G–LA (50, 200 μM) and VE (200 μM) on expression levels of proteins in PI3K-AKT and Nrf2-HO-1/NQO-1 signaling pathway. Different letters on the columns indicate significant differences ($p < 0.05$) between samples of different treatments for each protein.

Zheng: Conceptualization, Funding acquisition, Methodology, Project administration, Supervision, Validation, Writing – original draft, Writing – review & editing.

Declaration of Competing Interest

The authors declare that they have no known competing financial interests or personal relationships that could have appeared to influence the work reported in this paper.

Data availability

Data will be made available on request.

References

Bai, J., Zheng, Y., Wang, G., & Liu, P. (2016). Protective effect of D-Limonene against oxidative stress-induced cell damage in human lens epithelial cells *via* the p38 pathway. *Oxidative Medicine and Cellular Longevity, 2016*, 5962832.

Circu, M. L., & Aw, T. Y. (2010). Reactive oxygen species, cellular redox systems, and apoptosis. *Free Radical Biology and Medicine, 48*, 749–762.

Cruz, L., Benohoud, M., Rayner, C. M., Mateus, N., de Freitas, V., & Blackburn, R. S. (2018). Selective enzymatic lipophilization of anthocyanin glucosides from blackcurrant (*Ribes nigrum* L.) skin extract and characterization of esterified anthocyanins. *Food Chemistry, 266*, 415–419.

Cruz, L., Guimarães, M., Araujo, P., Evora, A., de Freitas, V., & Mateus, N. (2017). Malvidin 3-glucoside-fatty acid conjugates: From hydrophilic toward novel lipophilic derivatives. *Journal of Agricultural and Food Chemistry, 65*, 6513–6518.

Ershad, M., Shigenaga, M. K., & Bandy, B. (2021). Differential protection by anthocyanin-rich bilberry extract and resveratrol against lipid micelle-induced oxidative stress and monolayer permeability in Caco-2 intestinal epithelial cells. *Food & Function, 12*, 2950–2961.

Gao, S., Zhang, P., Zhang, C., Bao, F., Li, H., & Chen, L. (2018). Meroterpenoids from *Ganoderma sinense* protect hepatocytes and cardiomyocytes from oxidative stress induced injuries. *Fitoterapia, 131*, 73–79.

Gong, S., Fei, P., Sun, Q., Guo, L., Jiang, L., Duo, K., … Yun, X. (2021). Action mode of cranberry anthocyanin on physiological and morphological properties of *Staphylococcus aureus* and its application in cooked meat. *Food Microbioloy, 94*, Article 103632.

Gonçalves, A. C., Nunes, A. R., Falcão, A., Alves, G., & Silva, L. R. (2021). Dietary effects of anthocyanins in human health: A comprehensive review. *Pharmaceuticals, 14*, 690.

Guimarães, M., Pérez-Gregorio, M., Mateus, N., de Freitas, V., Galinha, C. F., Crespo, J. G., … Cruz, L. (2019). An efficient method for anthocyanins lipophilization based on enzyme retention in membrane systems. *Food Chemistry, 300*, Article 125167.

Harnly, J. (2017). Antioxidant methods. *Journal of Food Composition and Analysis, 64*, 145–146.

Je, J. Y., & Lee, D. B. (2015). *Nelumbo nucifera* leaves protect hydrogen peroxide-induced hepatic damage *via* antioxidant enzymes and HO-1/Nrf2 activation. *Food & Function, 6*, 1911–1918.

Jhan, J. K., Chung, Y. C., Chen, G. H., Chang, C. H., Lu, Y. C., & Hsu, C. K. (2016). Anthocyanin contents in the seed coat of black soya bean and their anti-human tyrosinase activity and antioxidative activity. *International Journal of Cosmetic Science, 38*, 319–324.

Jian, W., Chen, Y. H., Wang, L., Tu, L., Xiong, H., & Sun, Y. M. (2018). Preparation and cellular protection against oxidation of *Konjac* oligosaccharides obtained by combination of γ-irradiation and enzymatic hydrolysis. *Food Research International, 107*, 93–101.

Jiang, C., Sun, Z. M., Hu, J. N., Jin, Y., Guo, Q., Xu, J. J., … Wu, Y. S. (2019). Cyanidin ameliorates the progression of osteoarthritis *via* the Sirt6/NF-κB axis in vitro and *in vivo*. *Food & Function, 10*, 5873–5885.

Kensler, T. W., Wakabayashi, N., & Biswal, S. (2007). Cell survival responses to environmental stresses *via* the Keap1-Nrf2-ARE pathway. *Annual Review Pharmacology and Toxicology, 47*, 89–116.

Li, J., Zhao, R., Jiang, Y., Xu, Y., Zhao, H., Lyu, X., & Wu, T. (2020). Bilberry anthocyanins improve neuroinflammation and cognitive dysfunction in APP/PSEN1 mice *via* the CD33/TREM2/TYROBP signaling pathway in microglia. *Food & Function, 11*, 1572–1584.

Li, J., Wang, T., Liu, P., Yang, F., Wang, X., Zheng, W., & Sun, W. (2021). Hesperetin ameliorates hepatic oxidative stress and inflammation *via* the PI3K/AKT-Nrf2-ARE pathway in oleic acid-induced HepG2 cells and a rat model of high-fat diet-induced NAFLD. *Food & Function, 12*, 3898–3918.

Li, S., Tan, H. Y., Wang, N., Zhang, Z. J., Lao, L. X., Wong, C. W., & Feng, Y. B. (2015). The role of oxidative stress and antioxidants in liver diseases. *International Journal of Molecular Sciences, 16*, 26087–26124.

Lu, Y., Zhang, Y. Y., Hu, Y. C., & Lu, Y. H. (2014). Protective effects of 2',4' -dihydroxy-6'-methoxy-3',5'-dimethylchalcone against hydrogen peroxide-induced oxidative stress in hepatic L02 cell. *Archives of Pharmacal Research, 37*, 1211–1218.

Martínez-Hernández, A., Córdova, E. J., Rosillo-Salazar, O., García-Ortíz, H., Contreras-Cubas, C., Islas-Andrade, S., … Orozco, L. (2015). Association of HMOX1 and NQO1 polymorphisms with metabolic syndrome components. *PLoS One, 10*, e0123313.

Marquez-Rodriguez, A. S., Guimarães, M., Mateus, N., de Freitas, V., Ballinas-Casarrubias, M. L., Fuentes-Montero, M. E., … Cruz, L. (2021). Disaccharide anthocyanin delphinidin 3-*O*-sambubioside from *Hibiscus sabdariffa* L.: *Candida antarctica* lipase B-catalyzed fatty acid acylation and study of its color properties. *Food Chemistry, 344*, 12860.

Nomi, Y., Iwasaki-Kurashige, K., & Matsumoto, H. (2019). Therapeutic effects of anthocyanins for vision and eye health. *Molecules, 24*, 3311.

Poljsak, B., Šuput, D., & Milisav, I. (2013). Achieving the balance between ROS and antioxidants: When to use the synthetic antioxidants. *Oxidative Medicine and Cellular Longevity, 2013*, Article 956792.

Shi, J., & Zhao, X. H. (2019). Chemical features of the oligochitosan-glycated caseinate digest and its enhanced protection on barrier function of the acrylamide-injured IEC-6 cells. *Food Chemistry, 291*, 246–254.

Sinopoli, A., Calogero, G., & Bartolotta, A. (2019). Computational aspects of anthocyanidins and anthocyanins: A review. *Food Chemistry, 297*, Article 124898.

Tang, J. Y., He, A. H., Jia, G., Liu, G. M., Chen, X. L., Cai, J. Y., … Zhao, H. (2018). Protective effect of selenoprotein X against oxidative stress-induced cell apoptosis in human hepatocyte (LO2) cells *via* the p38 pathway. *Biological Trace Element Research, 181*, 44–53.

Teixeira, L. L., Pilon, G., Coutinho, C. P., Dudonné, S., Dube, P., Houde, V., … Hassimotto, N. (2021). Purple grumixama anthocyanins (*Eugenia brasiliensis* Lam.) attenuate obesity and insulin resistance in high-fat diet mice. *Food & Function, 12*, 3680–3691.

Thornberry, N. A., & Lazebnik, Y. (1998). Caspases: Enemies within. *Science, 281*, 1312–1316.

Tian, B., Zhao, J., Xie, X., Chen, T., Yin, Y., Zhai, R., … Li, J. (2021). Anthocyanins from the fruits of *Lycium ruthenicum* Murray improve high-fat diet-induced insulin resistance by ameliorating inflammation and oxidative stress in mice. *Food & Function, 12*, 3855–3871.

Vander Heiden, M. G., Chandel, N. S., Williamson, E. K., Schumacker, P. T., & Thompson, C. B. (1997). Bcl-xL regulates the membrane potential and volume homeostasis of mitochondria. *Cell, 91*, 627–637.

Wang, L., Zhu, L., Gao, S., Bao, F., Wang, Y., Chen, Y., … Chen, L. (2018). Withanolides isolated from *Nicandra physaloides* protect liver cells against oxidative stress-induced damage. *Journal of Functional Foods, 40*, 93–101.

Wei, T., Ji, X., Xue, J., Gao, Y., Zhu, X., & Xiao, G. (2021). Cyanidin-3-*O*-glucoside represses tumor growth and invasion in vivo by suppressing autophagy *via* inhibition of the JNK signaling pathways. *Food & Function, 12*, 387–396.

Wood, E., Hein, S., Heiss, C., Williams, C., & Rodriguez-Mateos, A. (2019). Blueberries and cardiovascular disease prevention. *Food & Function, 10*, 7621–7633.

Xia, T., Yao, J., Zhang, J., Zheng, Y., Song, J., & Wang, M. (2017). Protective effects of Shanxi aged vinegar against hydrogen peroxide-induced oxidative damage in LO2 cells through Nrf2-mediated antioxidant responses. *RSC Advances, 7*, 17377–17386.

Yang, W., Kortesniemi, M., Yang, B., & Zheng, J. (2018). Enzymatic acylation of anthocyanins isolated from alpine bearberry (*Arctostaphylos alpina*) and lipophilic properties, thermostability, and antioxidant capacity of the derivatives. *Journal of Agricultural and Food Chemistry, 66*, 2909–2916.

Yang, W., Kortesniemi, M., Ma, X., Zheng, J., & Yang, B. (2019). Enzymatic acylation of blackcurrant (*Ribes nigrum*) anthocyanins and evaluation of lipophilic properties and antioxidant capacity of derivatives. *Food Chemistry, 281*, 189–196.

Yang, X., Sun, H., Tu, L., Jin, Y., Wang, M., Liu, S., … He, S. (2020). Investigation of acute, subacute and subchronic toxicities of anthocyanin derived acylation reaction products and evaluation of their antioxidant activities *in vitro*. *Food & Function, 11*, 10954–10967.

Yin, Z., Guo, H., Jiang, K., Ou, J., Wang, M., Huang, C., … Ou, S. (2020). Morin decreases acrolein-induced cell injury in normal human hepatocyte cell line LO2. *Journal of Functional Foods, 75*, Article 104234.

Zeng, F., Zeng, H., Ye, Y., Zheng, S., Liu, J., Zhuang, Y., & Fei, P. (2021). Preparation of acylated blueberry anthocyanins through enzymatic method in aqueous/organic phase: Effects on its colour stability and pH-response characteristics. *Food & Function, 12*, 6821–6829.

Zhang, P., Liu, S., Zhao, Z., You, L., Harrison, M. D., & Zhang, Z. (2021). Enzymatic acylation of cyanidin-3-glucoside with fatty acid methyl esters improves stability and antioxidant activity. *Food Chemistry, 343*, Article 128482.

Zhou, P., Huang, C., Liu, F., Bai, W., Ou, S., & Zheng, J. (2021). Preparation and stability analysis of anthocyanin from black bean hull by enzymatic acylation. *Fine Chemicals, 38*, 1416–1422.